Drag Reduction Using Biomimetic Sharkskin Denticles

Dinesh Bhatia
School of Aerospace
University of Nottingham Ningbo China
Ningbo, China
dinesh.Bhatia@nottingham.edu.cn

Yingxue Zhao
School of Aerospace
University of Nottingham Ningbo China
Ningbo, China
zhaoyingxue1998@163.com

Devinder Yadav
School of Aerospace
University of Nottingham Ningbo China
Ningbo, China
Devinder.Yadav@nottingham.edu.cn

Jian Wang
Faculty of Science, Engineering and Computing
Kingston University
London, U.K.
J.Wang@kingston.ac.uk.

Abstract-This paper explores the use of sharkskin in improving the aerodynamic performance of aerofoils. A biomimetic analysis of the sharkskin denticles was conducted and the denticles were incorporated on the surface of a 2-Dimensional (2D) NACA0012 aerofoil. The aerodynamic performance including the drag reduction rate, lift enhancement rate, and Lift to Drag (L/D) enhancement rate for sharkskin denticles were calculated at different locations along the chord line of the aerofoil and at different Angles of Attack (AOAs) through Computational Fluid Dynamics (CFD). Two different denticle orientations were tested. Conditional results indicate that the denticle reduces drag by 4.3% and attains an L/D enhancement ratio of 3.6%.

Keywords-biomimetics; sharkskin denticles; flow control; drag reduction; CFD

I. INTRODUCTION

With the rapid growth of aviation in developing countries and the continuing growth of the existing aviation markets in developed countries, more people can enjoy air travels. The growing need for passengers has caused further environmental concerns since aircraft emissions can alter the atmospheric concentration of greenhouse gases that are related to climate change [1]. Moreover, economic concerns have been raised by airline companies. The supply of fossil fuels is limited and is depleting [2], therefore, much higher fuel prices and volatility occur [3]. The increase in jet fuel prices would increase air traffic and airport operation costs. Therefore, the aviation industry is focusing on environmental-friendly and green solutions to offset increasing fuel costs and higher carbon emissions. Drag reduction and improvement in aerodynamic efficiency is one way of reducing carbon emissions and fuel consumption [4].

Through the evolution of living organisms, there have been many examples in nature with traits which offer some insights into the design and optimization of engineering systems. The sharskin is one of these optimized structures. It has evolved to ensure that sharks can swim efficiently. Biomimetic analysis of the sharskin denticle structure has become a popular research topic. Biomimicry of the sharskin denticles has yielded drag reduction up to 10% compared with the corresponding smooth surface [5]. Applications inspired by the sharskin denticles have already been used in the Olympics. It was reported that the sharskin inspired speedo-swimsuit worn by Michael Phelps, the famous 8 times gold medals winner at the 2008 Olympics, helped in achieving 3-4% of drag reduction for swimmers [6]. This paper aims to investigate the impact of incorporating sharskin on 2D NACA0012 aerofoil by placing the denticles at strategic locations on the aerofoil. A detailed biomimetic study of the sharskin is conducted, following which the denticle sizing and modeling process are determined. Simulations are conducted and the results of sharskin on lift coefficient (cl), drag coefficient (cd), and L/D ratio at different positions along chord line at different AOAs are presented. Furthermore, the sharskin denticle working principle towards drag reduction and lift enhancement was analyzed to highlight the flow mechanism.

II. BIOMIMETIC STUDY OF SHARSKIN DENTICLES

Sharskin is one of the most popular bionic study topics for flow control and drag reduction and will be introduced in greater detail in this section. In order to observe the flow control mechanisms of sharskin denticles, the denticle geometry was first investigated. Sharskin is covered with rigid bony denticles. According to Figure 1(c), a sharskin denticle has a plate-like upper section with several ridges and narrows to a thin neck that roots into the skin [7]. The sharskin selected in this project belongs to a species of shortfin mako sharks called Isurus Oxyrinchus. This kind of shark is one of the fastest marine fish reaching a maximum speed of $70 km \cdot h^{-1}$ [8]. Some of the most detailed descriptions are shown in Figure 1 [7] and Table I [8].

Corresponding author: Dinesh Bhatia

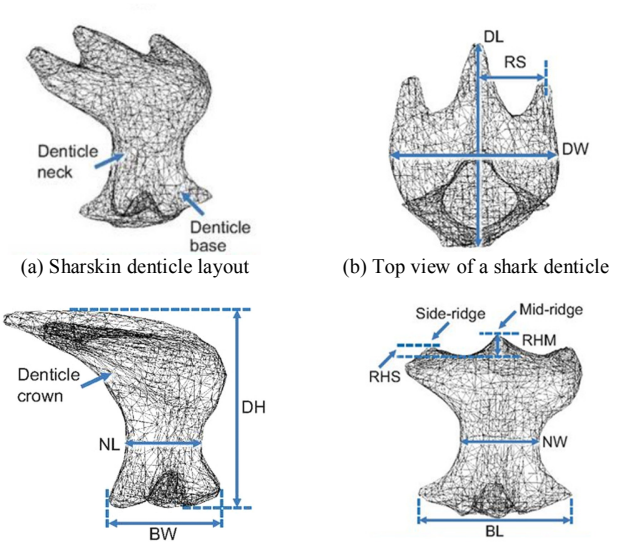

(a) Sharskin denticle layout (b) Top view of a shark denticle

(c) Side view of a shark denticle (d) Front view of a shark denticle

Fig. 1. Micro-CT scanned sharskin denticle geometry. Reproduced with permission from the Journal of Experimental Biology 217, 10 (2014). Copyright 2014 Company of Biologist Ltd. [7].

TABLE I. SHARSKIN DENTICLE PROTOTYPE DIMENSIONS [8]

Components	Dimensions (μm)
DL (denticle length)	151
DW (denticle width)	125
RS (spacing between adjacent ridges)	51
DH (denticle height)	113
BW (denticle base width)	119
NL (denticle neck length)	45.1
NW (denticle neck width)	50.9
BL (denticle base length)	83.8
RHM (height of middle ridge)	21
RHS (height of side ridge)	11

III. METHODOLOGY

The methodology adopted in this paper was divided into three aspects. Initially, the sharskin was modeled to ensure dynamic similarity and effective translation of the denticles from the hydrodynamic to an aerodynamic environment. Computational Aided Design (CAD) modeling of sharskin denticles was conducted and incorporated on the NACA0012 aerofoil. The CFD simulations of sharskin denticles and aerofoil were performed with ANSYS FLUENT.

A. Sizing of Sharskin Denticles

In order to quantify and analyze the sharskin aerodynamic properties, aerodynamic scaling was conducted to ensure that appropriate sizing of the shark-skin denticles could be incorporated on the aerofoil. Key dynamic similarity parameters such as the AOA, Mach Number (Ma), and Reynolds Number (Re) for the sharskin denticle model and real sharskin denticles should be computed to ensure their similarity [9]. Sizing was conducted with the aim to perform experimental testing of the sharskin denticle post numerical simulations. As a result, dynamic similarity exercise was conducted, keeping in mind the wind tunnel specifications, at the University of Nottingham Ningbo China (UNNC).

TABLE II. WIND TUNNEL SPECIFICATIONS AND SHARK HABITAT CONDITIONS

AF1300 wind tunnel UNNC	Isurus Oxyrinchus habitat and speed limit [10]
Temperature range: 5°C to 40°C	Prefers to inhabit in offshore waters with temperatures from 17 to 20°C
Nominal air velocity: 0 to 36m/s.	Maximum speed of 70km·h^{-1}.

According to the given specifications from the wind tunnel manual and shark habitat, it is noted that the maximum Ma in wind tunnel is less than 1, which means the effects of compressibility are very small, thereby Ma computation is no longer required. Therefore, by deriving the Re equations of the sharskin denticle model and the Re for real sharskin denticle prototype, given the known data of air and sea water density, shark velocity in seawater, air velocity designed in simulation, and the dynamic viscosity of sea water and air, the scale factor of sharskin denticle model dimensions versus the real sharskin denticle prototype dimensions were calculated. The derivation of equations is given below.

$$Re_\infty = \frac{\rho_\infty V_\infty l_\infty}{\mu_\infty} = Re_T = \frac{\rho_T V_T l_T}{\mu_T} \quad (1)$$

where Re_∞ is the Reynolds number for real shark denticles in sea water; Re_T is the Reynolds number for the shark denticle model in the air, ρ_∞ is the mean density of seawater at 17-20°C which is 1025.19kg/m^3 [10], ρ_T is the mean density of air at 20°C (1.2kg/m^3), V_∞ is the fastest velocity of Isurus Oxyrinchus (19.4m/s), V_T is the simulated air velocity (10m/s), μ_∞ is the mean viscosity of seawater at 17-20°C (0.001Pa/s), μ_T is the viscosity of air at 20°C (1.81×10^{-5}Pa/s), l_∞ is the height of the sharskin denticle prototype (DH=113×10^{-6}m) [7], and l_T is the height of the sharskin denticle model (m).

$$\text{scale factor} = \frac{l_T}{l_\infty} = \frac{\rho_\infty V_\infty \mu_T}{\rho_T V_T \mu_\infty} = 30 \quad (2)$$

Thus, when the wind speed was chosen to be 10m/s, the scale factor for shark denticle model dimension versus the real shark denticle dimension was calculated as 30 in (2). The detailed sharskin denticle model dimensions are listed in Table II.

TABLE III. SHARSKIN DENTICLE MODEL DIMENSIONS

Components	Dimensions (μm)
DL	4530
DW	3750
RS	1530
DH	3390
BW	3570
NL	1353
NW	1527
BL	2514
RHM	630
RHS	330

After calculating the sharskin denticle model dimensions, the modeling process using 3DExperience part design and generative wireframe & surface was performed. The sharskin denticle is shown in Figure 2 below.

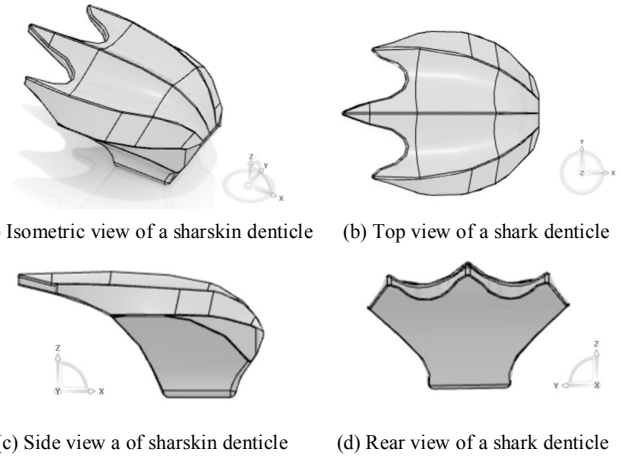

(a) Isometric view of a sharskin denticle (b) Top view of a shark denticle

(c) Side view a of sharskin denticle (d) Rear view of a shark denticle

Fig. 2. Sharskin denticle model geometry.

B. 2D simulation Setup and Validation

Once the sharskin and NACA0012 aerofoil were modeled, a comparative study was carried out between a standard NACA0012 aerofoil and the NACA0012 aerofoil with the sharskin denticles incorporated on it. The simulation case studies included 2D simulations of the NACA0012 aerofoil with the sharskin denticles put in the normal direction (as observed on the sharks) and NACA0012 aerofoil with the denticles put in the reverse direction as shown in Figure 3(c)-(d). The purpose of this simulation was to find the drag reduction rate, the L/D enhancement rate for the experiment group when sharkskin was put at different positions along the aerofoil chord line, and when the aerofoil was rotated at different AOAs. To eliminate the other factors that may interfere with the simulation results, all simulation settings were set to be the same for both the conventional aerofoil and the simulated denticle cases. An unstructured mesh of triangular shape throughout the control domain with 160,000 elements was chosen based on the mesh independent study. The mesh possesses high density elements clustered around the aerofoil surface as shown in Figure 3(a). The dimensions of the mesh and the boundary conditions were chosen from [11]. A C-shaped domain was used with the velocity inlet being placed at 10 times chord length (10c) from the aerofoil leading edge and 16c from the trailing edge. The height of the domain is 10c. The pressure outlet was placed 16c from the aerofoil trailing edge. A no-slip boundary condition was used for the aerofoil wall. Mesh elements were clustered around the aerofoil and denticle surface to ensure accurate resolution of flow features (Figure 3(b)). An inflation layer was adopted with a minimum first layer height of 5×10^{-7}m, 10 maximum layers, and a growth rate of 1.4 maintained from the aerofoil and denticle wall. A y+ value of 0.1 was maintained. All simulations were performed in ANSYS FLUENT. Solver settings were chosen based on [11]. The SST k-omega model was selected. It has shown great efficacy and accuracy in simulating micro-features at a scale similar to the sharskin denticles' and has accurately depicted the flow structure around these microfeatures [4]. As a result, the authors believe that the computational setup is suitable, reliable, and can accurately depict the flow features for the sharskin denticles and aerofoil presented in this paper.

TABLE IV. DETAILED COMPUTATIONAL SETUP

Grid	**Unstructured triangular 160,000 elements**
CFD Model	SST k-omega 2 Eqns
Solver	Steady state pressure based
Scheme	Second order coupled for pressure, momentum, and turbulence. Least square cell-based discretization for the gradient
Input parameters	Velocity: 10 ms−1, Turbulence intensity (Tu): 5%

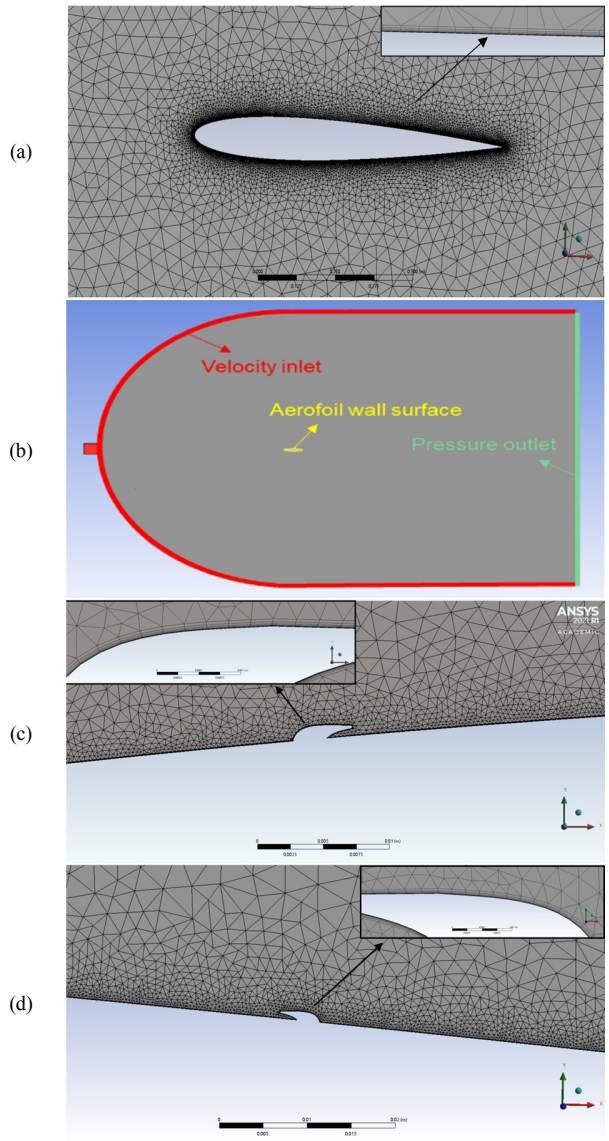

Fig. 3. Sharskin denticle model geometry. (a) NACA0012 control group, (b) simulation boundary conditions, (c) normal direction arrangement, (d) reverse direction arrangement

C. Validation and Reliability of Simulation Results

In order to ensure accurate simulation results, the result validation process was necessary, which included mesh independence check, benchmarking, and experimental result

verification. It was assured that the sharskin denticles were modeled, meshed, and simulated according to the standard procedure, and that the simulation results were reliable. The cd value was monitored as the number of mesh elements increased. It can be observed from Figure 4 that the number of elements increased from 0.2×10^5 to 1.6×10^5 before the condition of steady cd value was met. Thus, the corresponding element size of 0.003c was selected for edge mesh sizing, and 0.05c was chosen for body mesh sizing.

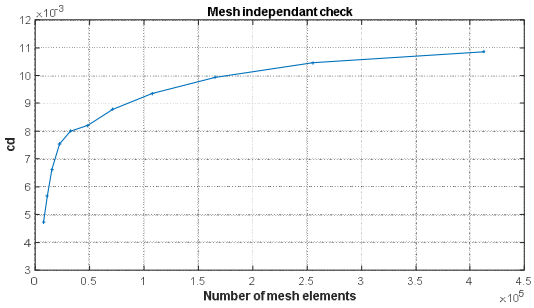

Fig. 4. Mesh independent check.

Moreover, the simulation data of cl and cd for smooth surface NACA0012 aerofoil was benchmarked with the existing data [11]. Figure 5 shows that the simulated results of cl and cd show good correlation with the existing simulation data.

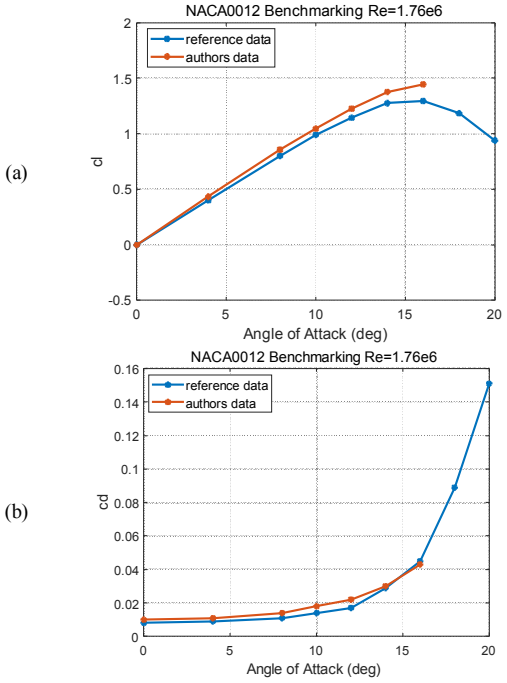

Fig. 5. Benchmarking results. (a) cl vs. AOA (°), (b) cd vs. AOA (°).

Lastly, the simulation results of NACA0012 aerofoil at Re=6×10^5 were compared with the X-Foil data at Re=6×10^5 [12]. Figure 6 shows that the cl and cd at different AOAs for the current study's simulation results are closely matched to the X-Foil data and show a very similar trend. Therefore, it can be concluded that the results presented for the NACA0012 aerofoil indicate reliability, repeatability, and accurate capture of the flow phenomenon by the applied simulation methods.

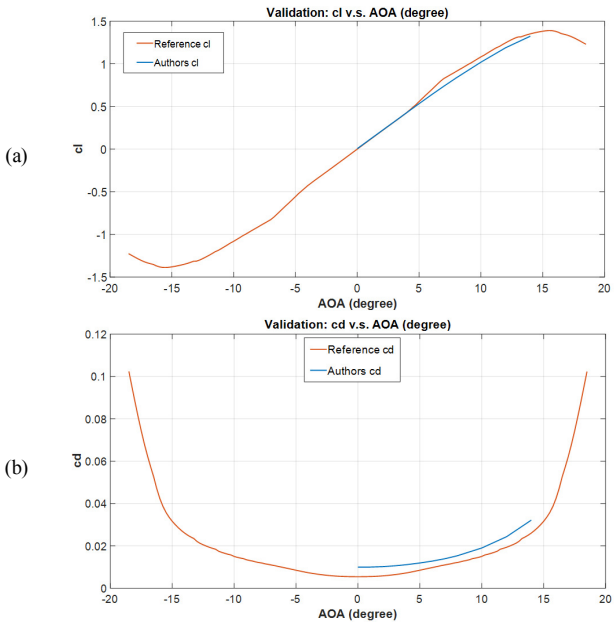

Fig. 6. Simulation verification with experimental data. (a) cl vs. AOA. (°), (b) cd vs. AOA (°).

IV. RESULTS AND DISCUSSION

A. Optimal Location of Sharskin Denticles

In this section, the simulation results of cl, cd, and L/D of sharskin denticles being put at normal and reverse directions are compared with the simulation results of a control group, i.e. NACA0012 aerofoil smooth surface at Re=6×10^5. The location of the denticles on chord line that has shown the highest amount of drag reduction and the highest amount of L/D enhancement is considered to be the optimal location of sharskin denticles.

1) Normal Direction Simulation Results

The denticles at normal direction were put on different locations, from 0.1c to 0.7c with a step change of 0.1c on NACA0012 aerofoil. Drag reduction rate, lift enhancement rate, and L/D enhancement rate were calculated and shown in Figures 7-9. Figures 7 and 9 show the drag reduction rate and L/D enhancement rate versus AOA (degrees). It is observed from Figures 7 and 9 that the optimal position of sharskin denticles at the normal direction on NACA0012 aerofoil for drag reduction and L/D enhancement is 0.16c, achieving maximum drag reduction and L/D enhancement of 3% and 1.5% achieved at 0° AOA and 4° AOA respectively. Moreover, it is observed from Figure 8 that the Lift enhancement rates for normal direction simulation at 1° to 2° AOA are all negative. At an AOA above 2°, the lift coefficient does not improve much, ranging between -1% to 1%. Furthermore, it was found

that for normal direction simulations, promising effects of drag reduction and L/D enhancement tend to occur when the denticles were put close to the leading edge and at low AOAs.

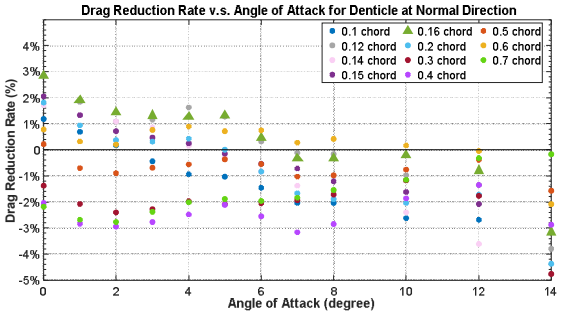

Fig. 7. Drag reduction rate vs. AOA for denticle at normal direction.

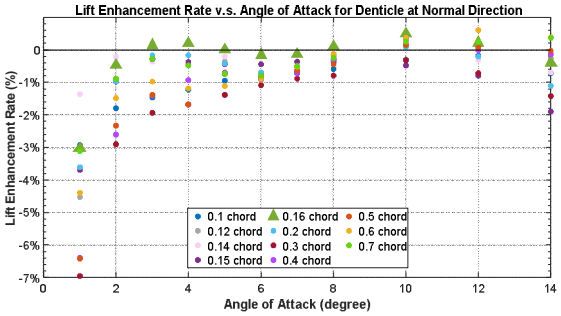

Fig. 8. Lift enhancement rate vs. AOA for denticle at normal direction.

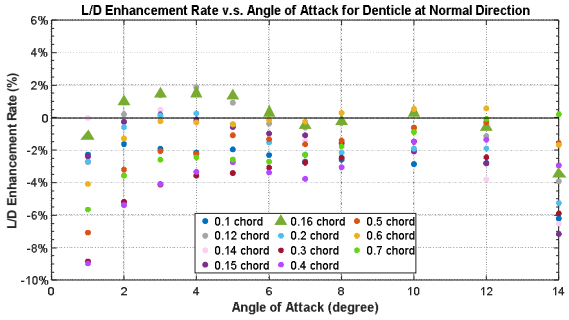

Fig. 9. L/D enhancement rate vs. AOA for denticle at normal direction.

2) Reverse Direction Simulation Results

Since the denticle placing in the normal direction in experiment group 1 is not very promising at higher AOAs, in order to further explore the performance of this denticle model in drag reduction and L/D enhancement, the sharskin denticles were put in the reverse direction to discover their effect. The sarkskin were put on different locations, from 0.1c to 0.7c on the NACA0012 aerofoil. The drag reduction coefficient, lift enhancement coefficient, and L/D enhancement coefficient of denticles placed in reverse direction were calculated and shown Figures 10-12.

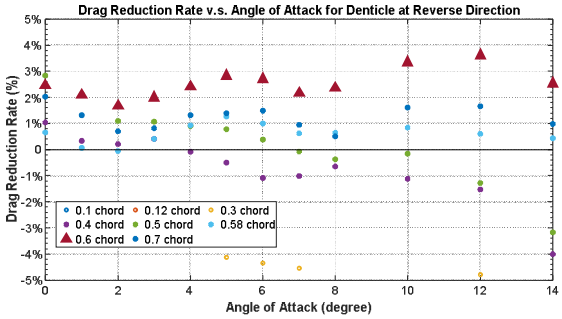

Fig. 10. Drag reduction rate vs. AOA at reverse direction.

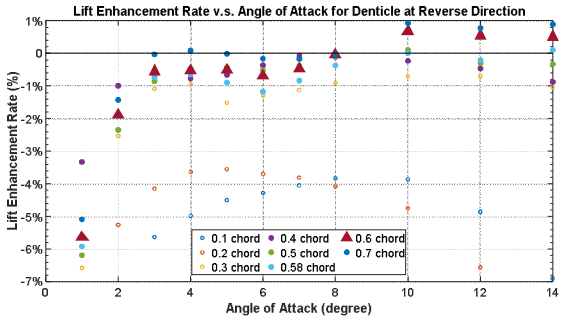

Fig. 11. Lift enhancement rate vs. AOA at reverse direction.

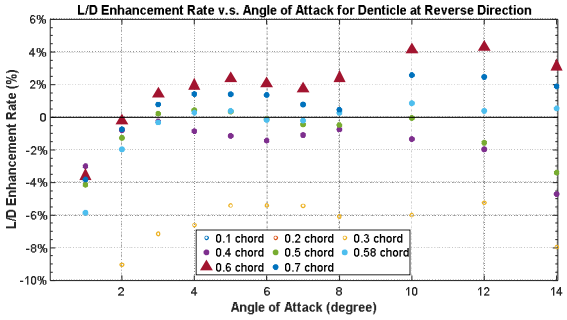

Fig. 12. L/D enhancement rate vs. AOA for denticle at reverse direction.

From Figures 10 and 12, the optimal position of sharskin at the reverse direction on NACA0012 aerofoil for drag reduction and L/D enhancement is found to be 0.6c. The maximum drag reduction and L/D enhancement for denticles placed in the reverse direction at 0.6c are 4.3% and 3.6% achieved both at 12° AOA. Moreover, the lift enhancement rate for reverse direction simulations varies from -1% to 1% after 2-degree AOA, as seen in Figure 11. Additionally, it was discovered that for the reverse direction arrangement, promising effects of drag reduction and L/D enhancement occur mostly when the denticles were placed close to the trailing edge at high AOAs.

B. Sharskin Denticle Flow Mechanism

Moreover, to find out the sharskin denticle drag reduction mechanism, the optimal solution of sharskin placed at the normal direction at 0.16c at 0° AOA and the optimal solution of sharskin in reverse direction at 0.6c at 12° AOA were compared with the control group of NACA0012 aerofoil at 0° and 12° AOA. The reason for this comparison was to make certain that the best scenario was analyzed.

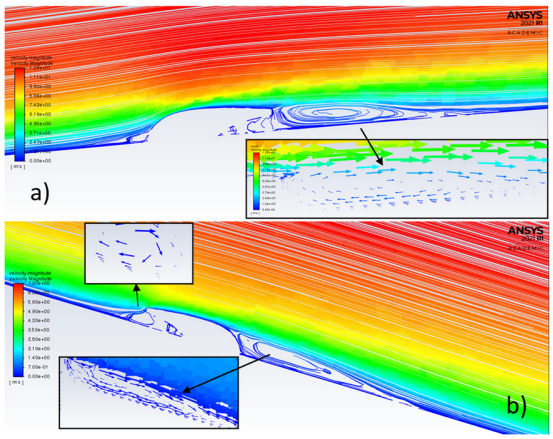

Fig. 13. Velocity magnitude pathline plot. (a) 0.16c normal direction at 0° AOA, (b) 0.6c reverse direction at 12° AOA.

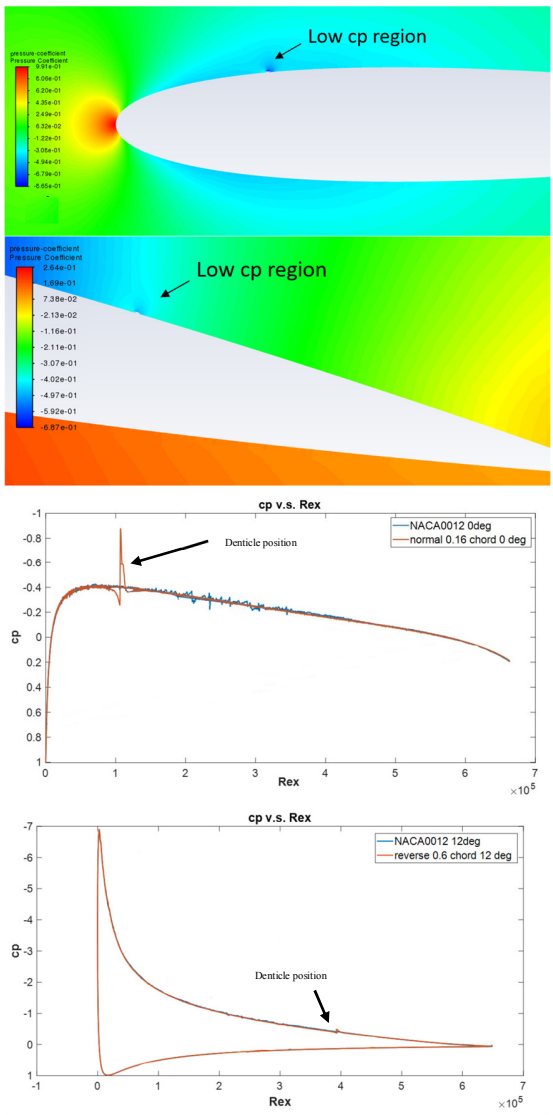

Fig. 14. Pressure coefficient contour plot and cp v.s. Rex plots. (a) 0.16c normal direction 0° AOA, (b) 0.6c reverse direction 12° AOA, (c) 0.16c normal direction 0° AOA, (d) 0.6c reverse direction 12° AOA.

The separation bubble at both the front and rear of the sharskin denticles are discovered from Figure 13. The separation bubble generated extra suction of airflow along the streamwise direction. Through the separation and reattachment of separation bubbles, the airflow accelerates and tends to stick closer to the aerofoil profile and thus it exhibits better aerodynamic performance. Moreover, from Figure 14(a)-(b), the denticles also generated a low-pressure zone at the top and downstream of the sharskin. The low-pressure zone has caused a greater pressure difference between the upper and lower surfaces of the aerofoil, which has a positive effect on lift enhancement. Meanwhile, since the pressure coefficient further downstream of the sharskin is bigger at the sharskin low-pressure zone, a favorable pressure difference along the streamwise direction is formed. This favorable pressure difference would eliminate some of the drag forces. This favorable pressure gradient can be numerically observed in Figure 14(c)-(d) where the cp for optimal solution of sharskin denticles is compared with the cp from the control group of NACA0012 smooth surface.

Additionally, the skin friction coefficient also suggested the drag reduction effect of sharskin denticles. It is observed from Figure 15(a)-(b) that the skin friction coefficient highly fluctuated in the NACA0012 control group. The skin friction coefficient after applying the sharskin is smoother than that from the control group at the same AOA, which suggests that the airflow was attached closer to the aerofoil surface after flowing through the sharskin denticles, causing less skin friction coefficient and less turbulent separation bubbles, therefore the aerodynamic efficiency of the aerofoil was improved.

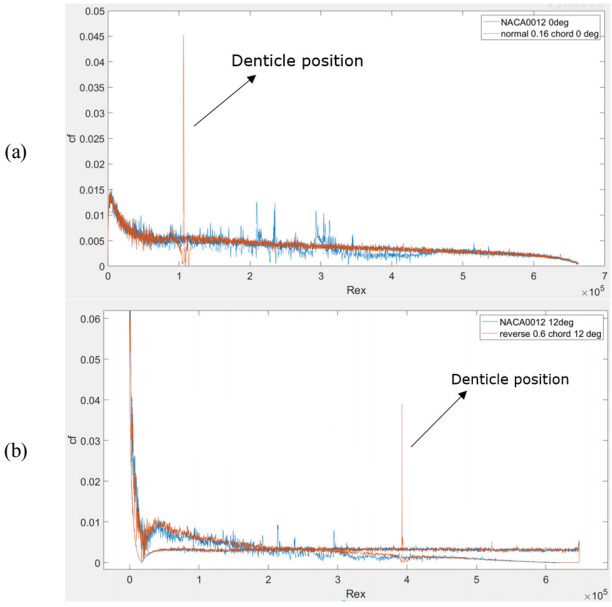

Fig. 15. Skin friction coefficient comparison with NACA0012 aerofoil. (a) 0.16c normal direction 0° AOA, (b) 0.6c reverse direction 12° AOA.

D. Undesired Pressure Gradient

Except from the sharskin denticle mechanism in drag reduction, an important feature of high-pressure region right upstream of the sharskin position was also noticed.

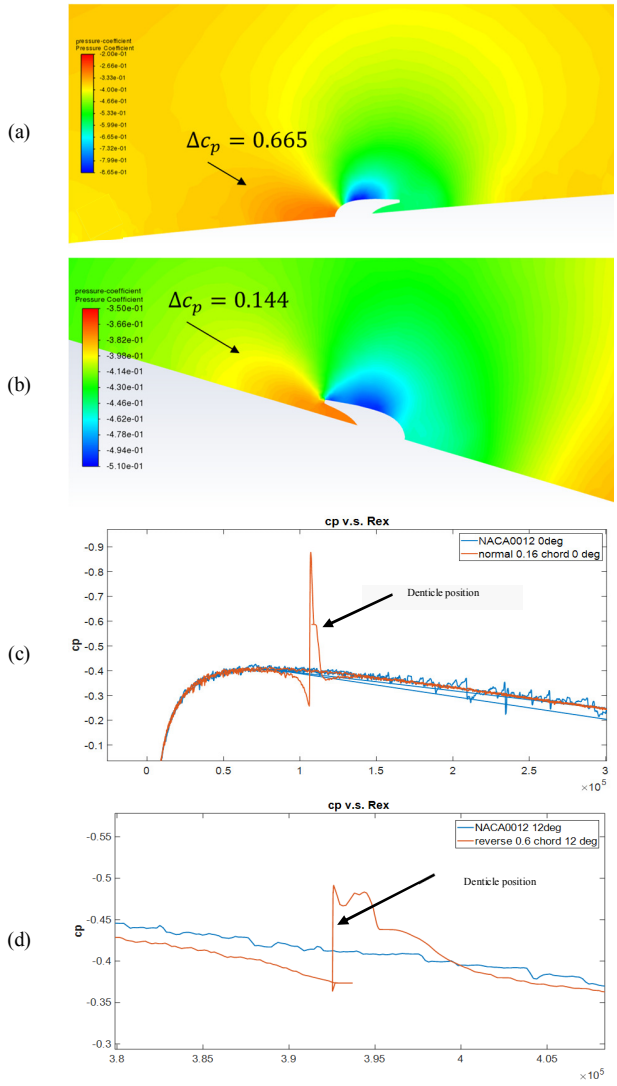

Fig. 16. Comparison between the optimal denticle simulation locations and NACA0012 control group. (a) Pressure coefficient contour, 0.16c normal direction 0° AOA, (b) pressure coefficient contour 0.6c reverse direction 12° AOA, (c) cp vs. Rex for normal direction 0.16c and NACA0012 at 0° AOA, (d) cp vs. Rex for reverse direction 0.6c and NACA0012 at 12° AOA.

According to Figure 16(a)-(b), the sharskin denticles at both normal and reverse directions have a high-pressure zone at the upstream of the sharskin which may be caused by the blockage phenomena of denticle frontal area when air flows through the denticles. This high-pressure zone would create an unfavorable pressure difference along the streamwise direction that tends to generate more drag, thus weakens the sharskin drag reduction effect. For the optimized case of normal direction in experimental group 1, the pressure difference is roughly 0.665 according to Figure 16(c), while for the optimized case of reverse direction in experimental group 2, the pressure difference is around 0.144 according to Figure 16(d). The higher the pressure difference between the upstream and downstream of sharskin is, the less drag reduction effect it would have. The reason why the reverse direction has a better drag reduction performance than the normal direction may be that the sharskin at reverse direction have a smaller unfavorable pressure difference compared to the normal direction case.

V. CONCLUSIONS

In this paper, simulations and wind tunnel experiments were conducted to attain drag reduction and L/D enhancement using strategically placed sharkskin within the laminar boundary layer. Based on the results, the following conclusions can be drawn:

- During the simulations, the maximum drag reduction and L/D enhancement, for normal direction and 0.16c sharskin position, are 3% and 1.5% achieved at 0° AOA and 4° AOA respectively. While the maximum drag reduction and L/D enhancement, for the reverse direction at 0.6c sharskin position, are 4.3% and 3.6% achieved both at 12° AOA.
- The presence of the sharskin denticles results in a favorable pressure gradient aft of the sharskin which leads to a damping of disturbances within the boundary layer. This leads to transition delay and drag reduction.
- The presence of the sharskin denticles also results in an undesired pressure gradient and weakens the drag reduction effect due to the blockage phenomena of sharskin frontal area.
- As the shape of the sharskin denticles has not been optimized, a study to identify an optimized the sharskin frontal area design closely would result in a smaller unfavorable pressure gradient and greater drag reduction.

ACKNOWLEDGEMENTS

The authors wish to thank the Ningbo Science and Technology Bureau for their funding under the Ningbo Natural Science Foundation program with project code: 2019A610116. The authors would also like to thank the University of Nottingham Ningbo China and Kingston University London.

REFERENCES

[1] D. A. Pamplona and C. J. P. Alves, "Civil Aircraft Emissions Study and Pollutant Forecasting at a Brazilian Airport," *Engineering, Technology & Applied Science Research*, vol. 10, no. 1, pp. 5217–5220, Feb. 2020, https://doi.org/10.48084/etasr.3227.

[2] A. A. Khaskheli, G. D. Walasai, A. S. Jamali, Q. B. Jamali, Z. A. Siyal, and A. Mengal, "Performance Evaluation of Locally-Produced Waste Cooking Oil Biodiesel with Conventional Diesel Fuel," *Engineering, Technology & Applied Science Research*, vol. 8, no. 6, pp. 3521–3524, Dec. 2018, https://doi.org/10.48084/etasr.2333.

[3] "U.S. Product Supplied for Crude Oil and Petroleum Products," *US Energy Information Administration*. https://www.eia.gov/dnav/pet/pet_cons_psup_dc_nus_mbbl_m.htm (accessed Sep. 10, 2021).

[4] D. Bhatia *et al.*, "Transition Delay and Drag Reduction using Biomimetically Inspired Surface Waves," *Journal of Applied Fluid Mechanics*, vol. 13, no. 4, pp. 1207–1222, Dec. 2019, https://doi.org/10.36884/jafm.13.04.30316.

[5] B. Dean and B. Bhushan, "Shark-skin surfaces for fluid-drag reduction in turbulent flow: a review," *Philosophical Transactions of the Royal Society A: Mathematical, Physical and Engineering Sciences*, vol. 368, no. 1929, pp. 4775–4806, Oct. 2010, https://doi.org/10.1098/rsta.2010.0201.

[6] G. D. Bixler and B. Bhushan, "Fluid Drag Reduction with Shark-Skin Riblet Inspired Microstructured Surfaces," *Advanced Functional Materials*, vol. 23, no. 36, pp. 4507–4528, 2013, https://doi.org/10.1002/adfm.201203683.

[7] L. Wen, J. C. Weaver, and G. V. Lauder, "Biomimetic shark skin: design, fabrication and hydrodynamic function," *Journal of Experimental Biology*, vol. 217, no. 10, pp. 1656–1666, May 2014, https://doi.org/10.1242/jeb.097097.

[8] F.-W. Patricia, D. Guzman, B. Iñigo, I. Urtzi, B. J. Maria, and S. Manu, "Morphological Characterization and Hydrodynamic Behavior of Shortfin Mako Shark (Isurus oxyrinchus) Dorsal Fin Denticles," *Journal of Bionic Engineering*, vol. 16, no. 4, pp. 730–741, Jul. 2019, https://doi.org/10.1007/s42235-019-0059-7.

[9] D. Bolster, R. E. Hershberger, and R. J. Donnelly, "Dynamic similarity, the dimensionless science," *Physics Today*, vol. 64, no. 9, pp. 42–47, Sep. 2011, https://doi.org/10.1063/PT.3.1258.

[10] F. L. Bachleda, *Dangerous Wildlife in California & Nevada: A Guide to Safe Encounters At Home and in the Wild*, 1st ed. Birmingham, AL, USA: Menasha Ridge Press, 2002.

[11] *Simulation CFD External Flow Validation: NACA 0012 Airfoil.* Autodesk, 2015.

[12] "Polars for NACA 0012 AIRFOILS (n0012-il)," *Airfoil Tools.* http://airfoiltools.com/airfoil/details?airfoil=n0012-il#polars (accessed Sep. 10, 2021).